Microcontact Printing of Gold Nanoparticle at Three-Phase Interface as Flexible Substrate for SERS Detection of MicroRNA

Hongying Li[1], Haina Zhang[1], Wei Luo[1], Ruo Yuan[1], Yingqi Zhao[2], Jian-An Huang[2*], Xia Yang[1*]

1 Key Laboratory of Luminescence Analysis and Molecular Sensing (Southwest University) Ministry of Education; College of Chemistry and Chemical Engineering, Southwest University, Chongqing, PR China

2 Faculty of Medicine, Faculty of Biochemistry and Molecular Medicine, University of Oulu, Aapistie 5A, 90220 Oulu, Finland

Abstract:

The rigidity of traditional solid-state surface-enhanced Raman spectroscopy (SERS) substrate hampers their application in the curved structure for nonplanar surface test and in-situ detection. Traditionally, the flexible Raman substrate is often prepared by transfer printing of patterned nanoparticles on the flexible materials such as polymer, paper, etc. However，the replicate patterns are often produced by high-cost instruments. In this study, a low-cost and flexible SERS substrate is prepared by using a microcontact printing technology to transfer a three-phase-assembled nanoparticle on a polydimethylsiloxane film, which can stabilize the assembled nanoparticles. Combining with the endonuclease Nt.BbvCI assisted amplification method, a SERS biosensor is constructed for microRNA 21 (miRNA 21) assay. This platform presents a wide dynamic range (100 fM ~1 nM), achieving a fabulous sensitivity with limit of detection of 11.96 fM for miRNA 21. Furthermore, after being bent 90° for 50 times, the Raman intensity of the flexible substrate shows a negligible change. This versatile flexible substrate exhibits considerable potential for SERS analysis, which also opens a new avenue for preparing flexible devices.

*Corresponding author.
E-mail address: Jianan.huang@oulu.fi (J-A. Huang), xiayang2@swu.edu.cn (X. Yang)

Keywords: SERS, flexible, microcontact printing, three-phase self-assembly, miRNA

1. Introduction

Surface-enhanced Raman spectroscopy (SERS) is an effective vibrational spectroscopy and the Raman scattering signals are enhanced by localized surface plasmon resonance (LSPR) on metal nanostructures. [1, 2] As a sensitive analytical technique ,[3-5] SERS are of significant interest for pharmaceutical diagnosis,[6] food security,[7] environmental monitoring,[8] interface science[9] and other fields. In recent years, various ordered plasmonic nanostructures on solid substrates including glass slides or silicon wafers have been developed to increase SERS signal reproducibility and sensitivity.[10, 11] Nevertheless, the solid substrates with inherent rigidity have some limit for special detection such as samples with complex topological shapes. Recently, flexible substrates, such as polymer[12-14] and paper-based SERS platform,[15-17] have advantages of softness, extensibility and optical transparency which can adhere to the curved structure for nonplanar surface test and in-situ detection.[18] For example, a wearable SERS biosensor of sweat molecules on human skin has been fabricated by nanoparticle array on a stretchable polymer film.[19] Traditionally, the flexible Raman substrates are often prepared by transfer printing of patterned nanoparticles on the flexible materials.[20, 21] However， the replicate patterns are often generated by high-cost instruments.[22]

Self-assembly of metal nanoparticles at the liquid interface[23, 24] has been proposed to fabricate ordered nanoparticle array as low-cost SERS substrates with good uniformity, but they cannot avoid the signal fluctuation.[25] To increase the repeatability of nanoparticle monolayers at large scale and overcome the shortcomings of solid-phase substrates, a strategy of combining liquid-phase assembly with a microcontact printing technique is proposed in this study. Microcontact printing is a microfabrication technology that prints graphics on a substrate through elastic stamps combined with self-assembled monolayer technology.[26]

MicroRNA (miRNA) is a class of non-coding endogenous single-stranded nucleic

acid small molecule that plays a vital role in cell differentiation and tissue development. Since their abnormal expression can trigger some diseases, they can serve as emerging tumor marker molecules. [27, 28] Thus, highly sensitive detection technology is urgently demanded. Due to the low abundance of miRNA, nucleic acid amplification techniques such as rolling circle amplification (RCA),[29] strand displacement amplification (SDA),[30] and catalytic hairpin assembly (CHA),[31] etc. have been used to improve the sensitivity of detection.

In this work, we fabricated a low-cost and flexible SERS substrate by transferring liquid-assembled nanoparticles at three-phase interface onto polydimethylsiloxane (PDMS) using a microcontact printing technique. Then the flexible substrate was employed for miRNA detection by combining enzymatic cleavage nucleic acid amplification strategy. The flexible sensor achieved a low limit of detection (LOD) of 11.96 fM. After being bent 90° for 50 times, the SERS detection sensitivity were not influenced. This work demonstrates a strategy for preparing flexible substrate, which shows a considerable potential SERS substrate in biosensing and flexible devices.

2. Experimental

All the chemical and reagent, apparatus, SERS measurement, sequence information of nucleic acid used in this experiment and experimental details can be found in the Supporting Information (SI).

2.1 Ligand exchange of hexadecyltrimethylammonium chloride (CTAC) coated nanoparticles.

1 mL gold nanosol was mixed with 9 mL water and centrifuged. Subsequently，1 mL polyvinyl pyrrolidone (PVP) solution (1 wt%, dissolving in ethanol) was added to the sediment and centrifuged to obtain PVP coated Au NPs. The sediment was redispersed in ethanol (1 mL) for subsequent use.

2.2 Self-assembly of Au NPs on three-phase interface.

200 μL Methylene chloride (CH_2Cl_2) and 200 μL PVP stabilized Au NPs solution was added into a hydrophobic centrifuge tube. Subsequently, 1 mL water and 200 μL of n-hexane was added along the wall of the container and the nanoparticles were driven

to the upper oil-water interface. Finally, a layer of brilliant mirror-like film was formed on the interface of water and n-hexane less than 1 min. After the upper oil phase was evaporated from the three-phase system, PDMS printed Au NPs film was used as SERS substrate.

2.3 Process of the cyclic amplification.

The process of connecting the magnetic beads with the ssDNA harpin H was provided by the SI. The procedure was performed in a total volume of 100 μL which contained 50 nM H, 50 nM S, 20 U Nt.BbvCI, 1× NE buffer 4 (20 mM tris(hydroxymethyl)aminomethane acetate salt (Tris-Ac), 10 mM magnesium acetate ($Mg(Ac)_2$), 50 mM potassium acetate (KAc), 1 mM dithiothreitol (DTT), pH 7.9) and varying concentrations of T. S, H, and T were incubated at 37°C for 2 hours to form a Y-shaped structure, and then Nt.BbvCI cleavage enzyme and buffer were added to react at 37°C for 1 hour. Finally, the enzyme was inactivated by placing the mixture at 80°C for 20 minutes.

2.4 The process of miRNA extraction from cells.

First, the cultured suspension cells were directly collected by centrifugation, and Buffer RL was added (add 500 μL Buffer RL for every less than 5×10^6 cells) and vortexed until there was no obvious cell agglomeration. The second step is to extract miRNA in an RNase-free environment. The details are in the SI.

3. Results and discussion

Scheme 1 A &B are a schematic diagram of the flexible biosensor. Specifically, Au NPs are assembled in a three-phase system to form Au layers on the upper water/oil interface. A flexible substrate was obtained by transferring the Au film with PDMS as a microcontact printing method.[32] Specifically, when the upper oil phase n-hexane was completely evaporated, the self-assembled two-dimensional Au film on the interface was vertically contacted and peeled off with a PDMS film. A cyclic magnification strategy triggered by the target of miRNA 21 is shown in part B. Hairpin probe (H) is decorated with ferrite bead (FB) and methylene blue (MB) at 5′and 3′ end, respectively. It is opened to form a Y-shaped structure in the presence of target probe

(T) and assistant probe (S), forming a recognition site of Nt.BbvCI enzymes. Nt.BbvCI, a nicking endonuclease, recognizes only one specific strand of double-stranded DNA. After being cleaved by the enzyme, the probe modified with MB (G) and the probe modified with FB are released. Then, the remaining part hybridizes with another H to trigger next cycle. Finally, after magnetic separation, supernatant droplet is added to the flexible film for detection. When more G is obtained, the Raman signal is stronger, achieving an amplified detection of miRNA.

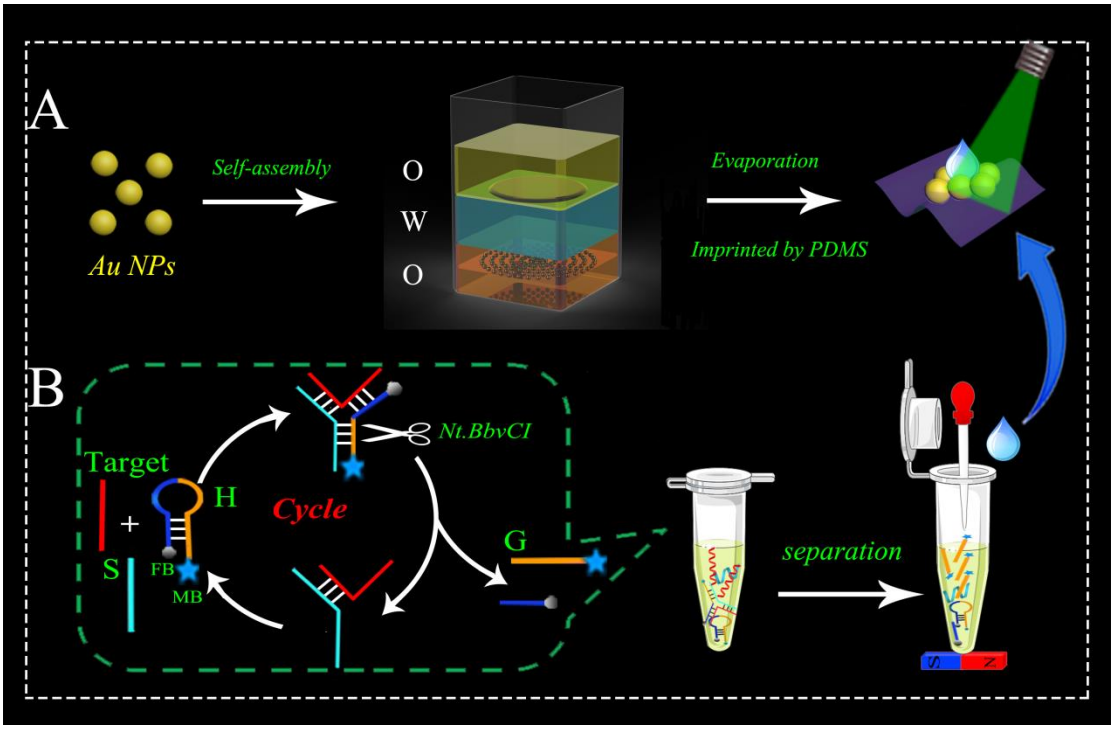

Scheme 1. Mechanism of the SERS Platform. (A) Au NPs self-assembly at the three-phase interface are microcontact printed by PDMS as a SERS substrate. (B) Enzymatic cleavage nucleic acid amplification strategy.

3.1 Characterization of materials and liquid phase interface.

The scanning electron microscopy (SEM) image is shown in Fig.1A, which displays that Au NPs are produced in high yield and exhibit many sharp thorns with the diameter of about 97 nm. The size distribution of Au NPs diameters is obtained by statistically measuring as shown Fig.1B.

The UV-vis spectrum (Fig.1C) illustrates that the absorption peak of Au seed and Au NPs are 525 nm and 640 nm, respectively, indicating that absorption wavelength would be red shifted significantly with the increase of particle size. What counts is that a lower surface charge of the larger-sized Au NPs that conduce to decrease the repulsive force

between the adjacent particles at the water /oil interface to assemble denser monolayers.[33] The front and top view of the self-assembly of Au NPs on the three-phase interface are shown in Fig. 1 (D & E). Supporting Video demonstrates the three-phase self-assembly process (Supporting Video). As seen from the video, CH_2Cl_2, PVP coated Au NPs and water was introduced sequentially to the hydrophobic centrifuge tube, a non-closely packed layers form at CH_2Cl_2/water interface. Nevertheless, once the n-hexane is added, Au NPs are promptly pulled into the water/n-hexane interface and form a dense monolayers film, and the whole process could be controlled within one minute. PVP coated Au NPs are crucial in this process because CTAC is an amphiphilic molecule, which make it difficult for Au NPs to assemble at the interface. Compared with the previous two-phase assembly (Supporting Video), this method can assemble faster, form a denser film without the addition of inducer. Moreover, the Marangoni force can overcome the electrostatic repulsion between particles. A gold film imprinted by PDMS (Fig.1F & G) shows that the film formed is relatively dense and uniform. In addition, we also used different amount of Au NPs with volume of 50, 75, 100, 125 and 150 μL (Fig.S1), respectively. They can all assemble in the three phases solution to form a dense metal film, indicating that the three-phase assembly method is not affected by the concentration of nanoparticles.

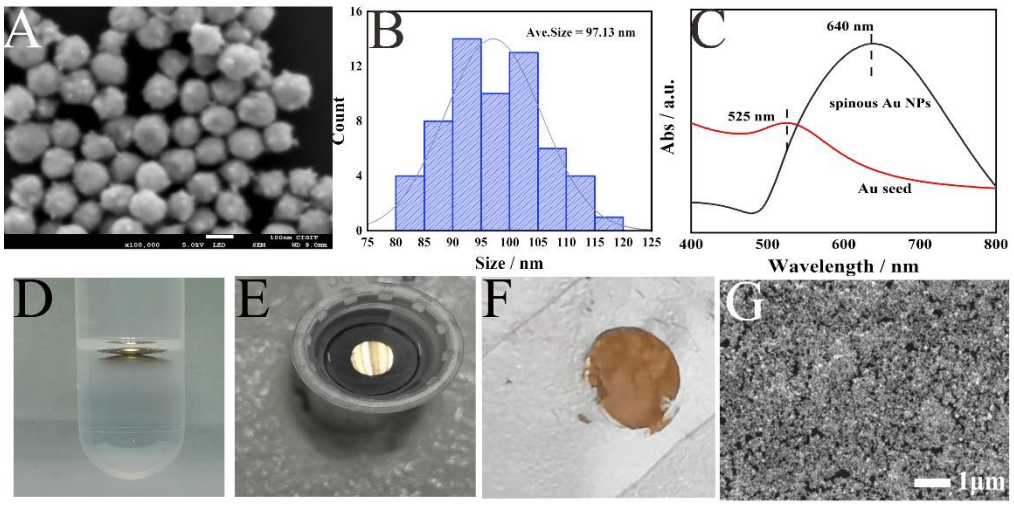

Fig. 1. (A) SEM image (B) Statistical graph of particle size distribution (C) UV-vis spectrum of Au NPs. Photograph of Au NPs assembled at the three-phase interface. (D) Front and (E) top views of the Au NPs on the three-phase interface. (F) Gold film on the interface imprinted by PDMS. (G) SEM image of the film.

A Raman mapping measurement of the Au NPs on PDMS on a 12 μm× 14 μm area with a step size of 1.5 μm× 2 μm was investigated to uncover uniformity of SERS signals. The image displayed in Fig. S2A is the corresponding intensity of the MB at 1623 cm^{-1} peak corresponding to the C-C stretching vibration of the thionine ring. In a random selected region, the Raman intensity at shift of 1623 cm^{-1} shows good signal uniformity with relative standard deviations (RSD) only 6.74% embodied in Fig. S2B.

3.2 Feasibility investigation of amplification validation.

To investigate the designed cycle amplification strategy, polyacrylamide gel electrophoresis (PAGE) experiment was conducted. As embodied in Fig. S3, Lane 1 is S and lane 2 is H. There are two bands in lane 3 (T and H) and lane 4 (S and H), affirming that the hairpin structure can't be opened only in the presence of T or S probe. A band with a lower migration rate appears in lane 5 that illustrates the hairpin is opened to form a Y-shaped (T-H-S) structure when both the T and S probe are present. In addition to verifying feasibility with PAGE, a Raman measurement was also demonstrated (Fig. S4) The distinct target-induced SERS signals at 1157 cm^{-1} ($\nu_{(C-N)}$), 1383 cm^{-1} ($\nu_{(C-N)}$) and 1623 cm^{-1}($\nu_{(C-C)ring}$) can be readily observed from MB molecular[34] (red line), which are due to formation of tremendous Y-type structure and numerous G probes released by enzymatic cleavage. As a comparison, there is small signal (blue line) when the target is not present in the circulating solution. The result shows that the target signal amplification strategy is successfully and effectively constructed.

3.3 Theory of Three-Phase Interface Assembly.

The minimization of the Helmholtz free energy is the intrinsic factors of interfacial assembly of nanoparticles. According to the reference,[35] the relationship between the energy (E) of a single particle and its vertical distance (z) to the water/ oil interface (as shown in Fig. 2A) can be expressed by the following，

$$E=\pi R^2\gamma_{O/W}\left[\left(\frac{Z}{R}\right)^2+2\left(\frac{\gamma_{P/O}}{\gamma_{O/W}}-\frac{\gamma_{P/W}}{\gamma_{O/W}}\right)\left(\frac{Z}{R}\right)+2\left(\frac{\gamma_{P/O}}{\gamma_{O/W}}+\frac{\gamma_{P/W}}{\gamma_{O/W}}\right)-1\right] \quad (1)$$

Where R is the effective radius of the Au NP, $\gamma_{o/w}$, $\gamma_{p/w}$, and $\gamma_{p/o}$ are the interfacial tensions between water/ oil, the particle /water, and the particle/oil, respectively.

As shown in Fig. 2B, if θ (the contact angle of the nanoparticle at the interface) is <90°, the particles are more hydrophilic. Whereas if θ > 90°, they are more hydrophobic. In accordance with the Young's equation

$$\cos\theta = \frac{\gamma_{P/O} - \gamma_{P/W}}{\gamma_{O/w}} \quad (2)$$

While, the minimum in E (E_{min}) occurs when

$$z = \frac{\gamma_{P/W} - \gamma_{P/O}}{\gamma_{O/W}} R \quad (3)$$

From equations (2) and (3), $z = -R\cos\theta$, it is not difficult to find that only when the angle θ = 90° can Au NPs stabilize at the water/ oil interface. Therefore, $\gamma_{P/0} = \gamma_{P/W}$. Logically, the minimum interfacial energy E_{min} can be expressed as

$$E_{min} = \pi R^2 \left(4\gamma_{P/O} - \gamma_{O/W}\right) \quad (4)$$

Consequently, as individual particles migrate from the lower dichloromethane oil phase to the upper n-hexane oil phase, the change of the interface energy (ΔE) is expressed as

$$\Delta E = E_{min} - E_{P/O} = -\frac{\pi R^2}{\gamma_{O/W}}\left[\gamma_{O/W} - \left(\gamma_{P/W} - \gamma_{P/O}\right)\right]^2 = -\pi R^2 \gamma_{O/W} \quad (5)$$

The three-phase system may be depicted as in Fig. 2C, the upper and lower oil/water interfaces are formed. Eventually, the Au NPs stabilize at the upper interface. The change of the interface energy (ΔE_1) in this migration process is described as

$$\Delta E_1 = E_{upp} - E_{low} = -\pi R^2 \left(\gamma_{O_{upp}/W} - \gamma_{O_{low}/W}\right) = -\pi R^2 \Delta\gamma \quad (6)$$

From the above conclusion, it is clear that the difference of surface tension between the two oil/water interfaces is the driving force for the migration of nanoparticles, and the decrease of interface free energy is also attributed to this.

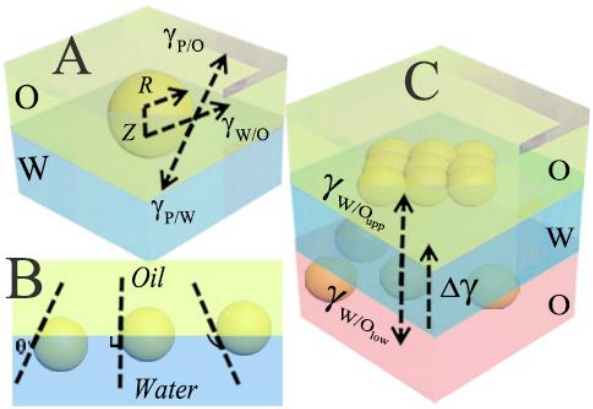

Fig. 2. (A) Schematic diagram of calculation of interface energy. (B) Position of a single particle at a planar oil/water interface for a contact angle measured through the aqueous phase less than 90° (left), equal to 90° (center), and greater than 90° (right). (C) Illustration of differences in surface tension driving the migration of nanoparticles in a three-phase system.

3.4 Optimization of Assay Conditions.

Enzyme concentrations and target incubation time were optimized for the development of better performance biosensors. Specifically, the SERS response was examined with six different Nt.BbvCI concentrations of 0.05, 0.10, 0.15, 0.20, 0.25 and 0.30 $U\mu L^{-1}$, respectively. As shown in Fig. 3A&B, when the concentrations of Nt.BbvCI ranges from 0.05 to 0.20 UμL-1, the Raman intensity gradually enhances, while the intensity decreases as the concentration of Nt.BbvCI from 0.20 to 0.30 $U\mu L^{-1}$. This is due to the van der Waals force effect between the Nt.BbvCI and Au NPs. [36]Thus, the optimized concentration of enzyme was chosen to be 0.20 $U\mu L^{-1}$ for the subsequent SERS experiments. As shown in Fig. 3C&D, with the increase of incubation time from 0.5 h to 3.0 h, the intensity gradually rises and then achieves a plateau at 2 h, indicating that the reaction in the system reaches equilibrium. Therefore, the optimal incubation time is chosen to be 2 h.

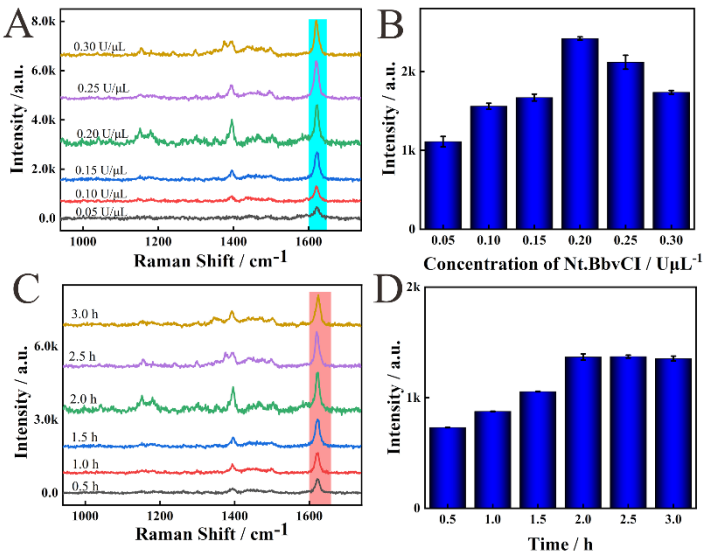

Fig. 3. (A) Raman spectra on the flexible substrate after the upper solution with different concentrations of Nt.BbvCI enzyme added and (B) the corresponding intensities of Raman shift at 1623 cm^{-1} (n=3). (C) Raman spectra on the flexible substrate after the upper solution with different incubation time of the target added and (D) the corresponding intensities of Raman shift at 1623 cm^{-1} (n=3).

3.5 SERS analysis of miRNA 21

MiRNA 21 was used to assess the SERS performance of this designed biosensor under the optimal analysis conditions (1× NE buffer 4: 20 mM Tris-Ac, 10 Mm $Mg(Ac)_2$, 50 mM KAc, 1 mM DTT, pH 7.9). Obviously, the SERS intensity at Raman shift of 1623 cm^{-1} enhances gradually with the growth concentrations of miRNA 21 in the range from 100 fM to 1 nM shown in Fig. 4A. A positive linear relationship is described between the corresponding SERS intensities (y) and the logarithm concentrations of miRNA 21 (lg c) in Fig. 4B. The regression equation was expressed as y = 232.5lg c-185.1 (R^2=0.993). The R^2 indicates the sensor's reliable performance for quantitative analysis in its linear range. The LOD of this SERS platform is 11.96 fM(details are in supporting information), which is among the highest sensitivity achieved by SERS substrates according to our knowledge. As can be seen from Table 1, compared with other works, the results point out this SERS biosensor provides good performance for miRNA 21 detection.

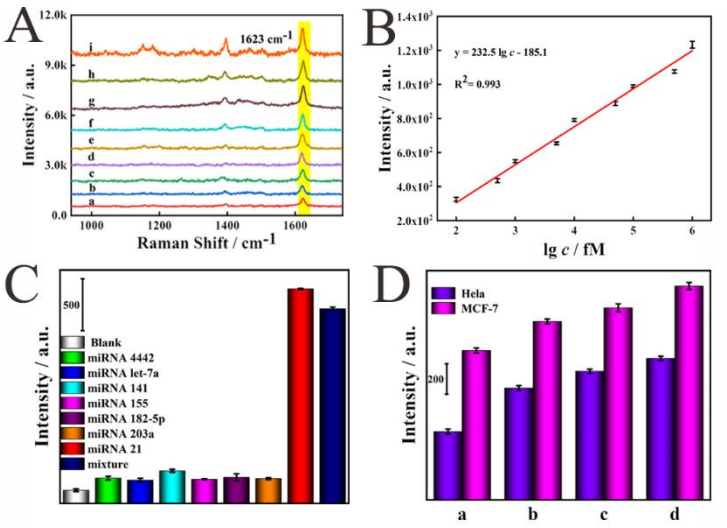

Fig. 4. (A) Raman spectra of the SERS biosensor with a series of concentrations of miRNA 21 [from a to i: (a) 1 $\times 10^2$, (b) 5×10^2, (c) 1×10^3, (d) 5×10^3, (e) 1×10^4, (f) 5×10^4, (g) 1×10^5, (h) 5×10^5, (i) 1×10^6(fM)], and (B) corresponding linear regression equation of the miRNA 21 detection(n=3). (C) SERS response of the fabricated biosensor toward miRNA 21 compared with other six types of miRNAs (n=3). The concentrations of these are 1 nM, respectively. (D) SERS response of the proposed biosensor with different concentration of MCF-7 and HeLa cells (a) 10^2, (b) 10^3, (c) 10^4 and (d) 10^5 cells (n=3).

3.6 Selectivity and application.

To further characterize the selectivity of SERS biosensor, it was incubated with target miRNA 21(100 pM) and six other interferences including miRNA 4442(1 nM), miRNA-let-7a (1 nM), miRNA 141(1 nM), miRNA 155(1 nM), miRNA 182-5p (1 nM) and miRNA 203a (1 nM). From Fig. 4C, it can be found that the SERS intensity of the six interferers is close to that of the blank sample. The intensity is also negligible compared to that with the target miRNA 21 and its mixture. The results of this analysis can be fully elucidated the prominent selectivity toward miRNA 21.

To further testify the sensor performance for detection in mixture environment, miRNA in cell lysates were measured. After cell counting, lysates of cervical cancer cells (Hela) and human breast cancer cells (MCF-7) treated with the RNA extraction kit. The extracted cell lysate replaced the target and participated in the nucleic acid amplification cycle. As exhibited in Fig. 4D, the relative SERS intensity increases gradually as the growth of MCF-7 cell concentration (from 10^2 to 10^5 cells). While under equal analysis conditions, a lower SERS response is obtained when incubated with the lysate of HeLa cell, which is due to that miRNA 21 is less expressed in HeLa cells compared with that in MCF-7 cell. These experimental results are consistent with

those reported in previous literature.[37] Hence, the constructed biosensor stands a chance of application in clinical diagnosis for miRNA 21 detection.

3.7 Stability of flexible SERS sensor.

To evaluate the mechanical durability of flexible sensors, the mechanical stimuli of bends tests were performed. After being bent 90° for 50 times, no obvious crack of the substrate was found in Fig. 5A, indicating that it had excellent toughness. Then, the SERS intensity was recorded for miRNA (1 nM) on the sensor after each mechanical deformation. During the 50 times of mechanical bending, the Raman intensity of the shift at 1623 cm^{-1} exhibits a negligible change in Fig. 5B & C, which shows that the flexible sensor constructed by this method has excellent stability.

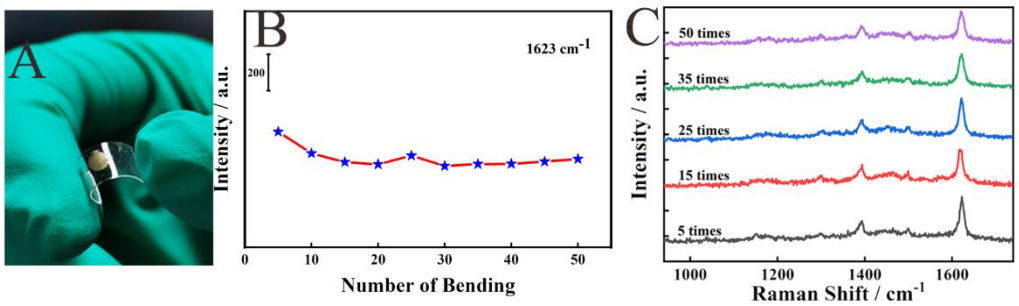

Fig. 5. (A) The photo of flexible SERS substrate. (B) SERS intensity change chart collected of Raman shift at 1623 cm^{-1} for 50 times; (C) the corresponding Raman spectrum of (B).

To test the stability and reproducibility of the SERS substrate, the following parallel tests were performed. Fig. 6A depicts the Raman spectra of 10 different points of one SERS platform, and the RSD of the SERS intensity at 1623 cm^{-1} in those platforms is 1.62% (Fig. 6B). Furthermore, 5 parallel SERS platforms with the same miRNA 21 concentration are shown in Fig. 6C and the RSD is 7.17% (Fig. 6D). The results substantiate that the SERS platform possesses excellent reproducibility and stability.

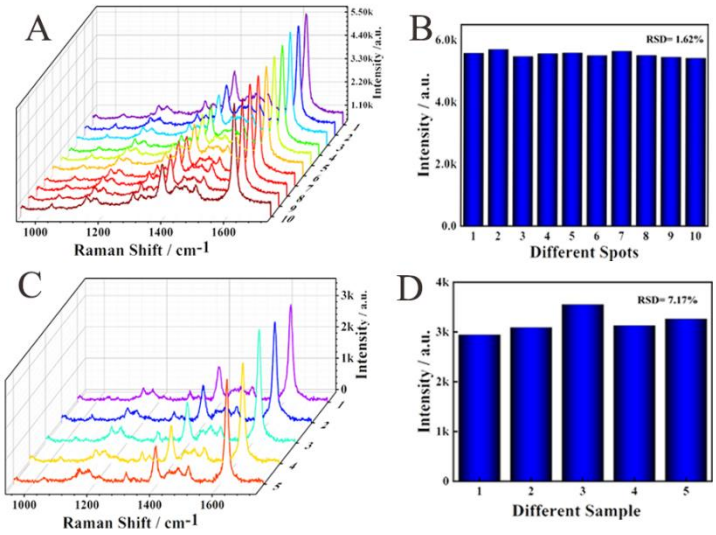

Fig.6. (A) Raman spectra and (B) bar statistics of Raman shift at 1623 cm $^{-1}$ of 10 randomly collected points on the same sample. The miRNA 21 concentration is 50 nM. (C) Raman spectra and (D) bar statistics of Raman shift at 1623 cm $^{-1}$ of 5 different platforms on the same assay conditions. The concentration of miRNA 21 is 10 nM.

Table1. Comparison of Other Studies for miRNA 21 Detection

analytical method	LOD	linear range	refs.
ECL	0.3 pM	1 pM~10 nM	[38]
SERS	0.11 nM	4 nM ~ 1.2×10^3 nM	[39]
SERS	2.72 pM	10 pM ~ 10 nM	[40]
SERS	0.15 pM	5 pM ~ 10^2 nM	[41]
SERS	166 fM	1 pM ~ 10 nM	[42]
SERS	11.96 fM	10^2 fM ~ 1 nM	This work

4. Conclusions

In this work, we propose a low-cost strategy to microcontact printing the Au NPs on the three-phase interface and obtain a flexible SERS substrate, which shows a remarkable sensitive SERS performance with a wide dynamic range (100 fM ~1 nM) for detection of miRNA. This work can provide a new idea for low-cost and large-scale fabrication of flexible materials for SERS analysis and flexible devices applications. However, considering the printing of nanoparticles on flexible substrates, the hot spots would be destroyed in the substrate in complex environment such as long time soak. We will use DNA nanostructures or chemical molecular to stabilize the nanoparticles

in the further works.

CRediT authorship contribution statement

Hongying Li: Conceptualization, Methodology, Formal analysis, Investigation, Writing - Original Draft, Visualization. **Haina Zhang &Wei Luo**: Formal analysis, Data curation. **Yingqi Zhao**: Investigation, Conceptualization. **Ruo Yuan**: Supervision, Conceptualization. **Jian-An Huang& Xia Yang**: Project administration, Funding acquisition, Writing – review & editing.

Declaration of competing interest

The authors declare no competing financial interest.

Acknowledgments

This work is supported by the National Natural Science Foundation of China (22174114). Jian-An Huang acknowledges the DigiHealth-project, a strategic profiling project at the University of Oulu that is supported by the Academy of Finland (project number 326291) and the University of Oulu.

Appendix A. Supplementary data

Supplementary data to this article is attached as SI.

References

[1] G. Barbillon, Latest Novelties on Plasmonic and Non-Plasmonic Nanomaterials for SERS Sensing, Nanomaterials, 10 (2020) 1200.

[2] S. Schluecker, Surface-Enhanced Raman Spectroscopy: Concepts and Chemical Applications, Angewandte Chemie-International Edition, 53 (2014) 4756-4795.

[3] H.X. Xu, E.J. Bjerneld, M. Kall, L. Borjesson, Spectroscopy of single hemoglobin molecules by surface enhanced Raman scattering, Physical Review Letters, 83 (1999) 4357-4360.

[4] S. Sevim, C. Franco, X.-Z. Chen, A. Sorrenti, D. Rodriguez-San-Miguel, S. Pane, A.J. deMello, J. Puigmarti-Luis, SERS Barcode Libraries: A Microfluidic Approach, Advanced Science, 7 (2020) 1903172.

[5] C. Zhu, G. Meng, P. Zheng, Q. Huang, Z. Li, X. Hu, X. Wang, Z. Huang, F. Li, N. Wu, A Hierarchically Ordered Array of Silver-Nanorod Bundles for Surface-Enhanced Raman Scattering Detection of Phenolic Pollutants, Advanced Materials, 28 (2016) 4871-4876.

[6] S. McAughtrie, K. Faulds, D. Graham, Surface enhanced Raman spectroscopy (SERS): Potential applications for disease detection and treatment, Journal of Photochemistry and Photobiology C-Photochemistry Reviews, 21 (2014) 40-53.

[7] T. Yaseen, H. Pu, D.-W. Sun, Functionalization techniques for improving SERS substrates and their applications in food safety evaluation: A review of recent research trends, Trends in Food Science & Technology, 72 (2018) 162-174.

[8] X. Li, G. Chen, L. Yang, Z. Jin, J. Liu, Multifunctional Au-Coated TiO2 Nanotube Arrays as Recyclable

SERS Substrates for Multifold Organic Pollutants Detection, Advanced Functional Materials, 20 (2010) 2815-2824.
[9] F. Reincke, S.G. Hickey, W.K. Kegel, D. Vanmaekelbergh, Spontaneous assembly of a monolayer of charged gold nanocrystals at the water/oil interface, Angewandte Chemie-International Edition, 43 (2004) 458-462.
[10] S. Lin, X. Lin, Y. Liu, H. Zhao, W. Hasi, L. Wang, Self- assembly of Au@ Ag core- shell nanocubes embedded with an internal standard for reliable quantitative SERS measurements, Analytical Methods, 10 (2018) 4201-4208.
[11] J.-A. Huang, Y.-Q. Zhao, X.-J. Zhang, L.-F. He, T.-L. Wong, Y.-S. Chui, W.-J. Zhang, S.-T. Lee, Ordered Ag/Si Nanowires Array: Wide-Range Surface-Enhanced Raman Spectroscopy for Reproducible Biomolecule Detection, Nano Letters, 13 (2013) 5039-5045.
[12] X. Liu, J. Ma, P. Jiang, J. Shen, R. Wang, Y. Wang, G. Tu, Large-Scale Flexible Surface-Enhanced Raman Scattering (SERS) Sensors with High Stability and Signal Homogeneity, Acs Applied Materials & Interfaces, 12 (2020) 45332-45341.
[13] Z. Li, G. Meng, Q. Huang, X. Hu, X. He, H. Tang, Z. Wang, F. Li, Ag Nanoparticle-Grafted PAN-Nanohump Array Films with 3D High-Density Hot Spots as Flexible and Reliable SERS Substrates, Small, 11 (2015) 5452-5459.
[14] P. Kumar, R. Khosla, M. Soni, D. Deva, S.K. Sharma, A highly sensitive, flexible SERS sensor for malachite green detection based on Ag decorated microstructured PDMS substrate fabricated from Taro leaf as template, Sensors and Actuators B-Chemical, 246 (2017) 477-486.
[15] W.-L.-J. Hasi, S. Lin, X. Lin, X.-T. Lou, F. Yang, D.-Y. Lin, Z.-W. Lu, Rapid fabrication of self-assembled interfacial film decorated filter paper as an excellent surface-enhanced Raman scattering substrate, Analytical Methods, 6 (2014) 9547-9553.
[16] M. Park, H. Jung, Y. Jeong, K.-H. Jeong, Plasmonic Schirmer Strip for Human Tear-Based Gouty Arthritis Diagnosis Using Surface-Enhanced Raman Scattering, Acs Nano, 11 (2017) 438-443.
[17] S. Lin, W. Hasi, S. Han, X. Lin, L. Wang, A dual-functional PDMS-assisted paper-based SERS platform for the reliable detection of thiram residue both on fruit surfaces and in juice, Analytical Methods, 12 (2020) 2571-2579.
[18] D. Zhang, H. Pu, L. Huang, D.-W. Sun, Advances in flexible surface-enhanced Raman scattering (SERS) substrates for nondestructive food detection: Fundamentals and recent applications, Trends in Food Science & Technology, 109 (2021) 690-701.
[19] Y. Wang, C. Zhao, J. Wang, X. Luo, L. Xie, S. Zhan, J. Kim, X. Wang, X. Liu, Y. Ying, Wearable plasmonic-metasurface sensor for noninvasive and universal molecular fingerprint detection on biointerfaces, Science Advances, 7 (2021) eabe4553.
[20] H. Liu, Y. He, K. Cao, Flexible Surface-Enhanced Raman Scattering Substrates: A Review on Constructions, Applications, and Challenges, Advanced Materials Interfaces, 8 (2021) 2100982.
[21] K. Xu, R. Zhou, K. Takei, M. Hong, Toward Flexible Surface-Enhanced Raman Scattering (SERS) Sensors for Point-of-Care Diagnostics, Advanced Science, 6 (2019) 1900925.
[22] A. Perl, D.N. Reinhoudt, J. Huskens, Microcontact Printing: Limitations and Achievements, Advanced Materials, 21 (2009) 2257-2268.
[23] W. Wei, Y. Wang, J. Ji, S. Zuo, W. Li, F. Bai, H. Fan, Fabrication of Large-Area Arrays of Vertically Aligned Gold Nanorods, Nano Letters, 18 (2018) 4467-4472.
[24] Z. Wang, M. Li, W. Wang, M. Fang, Q. Sun, C. Liu, Floating silver film: A flexible surface-enhanced Raman spectroscopy substrate for direct liquid phase detection at gas-liquid interfaces, Nano

Research, 9 (2016) 1148-1158.
[25] W. Luo, C. Wu, S. Huang, X. Luo, R. Yuan, X. Yang, Liquid Phase Interfacial Surface-Enhanced Raman Scattering Platform for Ratiometric Detection of MicroRNA 155, Analytical Chemistry, 92 (2020) 15573-15578.
[26] E.P. Yalcintas, K.B. Ozutemiz, T. Cetinkaya, L. Dalloro, C. Majidi, O.B. Ozdoganlar, Soft Electronics Manufacturing Using Microcontact Printing, Advanced Functional Materials, 29 (2019) 1906551.
[27] A. Válóczi, C. Hornyik, N. Varga, J. Burgyán, S. Kauppinen, Z. Havelda, Sensitive and specific detection of microRNAs by northern blot analysis using LNA-modified oligonucleotide probes, Nucleic acids research, 32 (2004) e175-e175.
[28] C. Chen, D.A. Ridzon, A.J. Broomer, Z. Zhou, D.H. Lee, J.T. Nguyen, M. Barbisin, N.L. Xu, V.R. Mahuvakar, M.R. Andersen, K.Q. Lao, K.J. Livak, K.J. Guegler, Real-time quantification of microRNAs by stem-loop RT-PCR, Nucleic acids research, 33 (2005) e179-e179.
[29] J. Banér, M. Nilsson, M. Mendel-Hartvig, U. Landegren, Signal amplification of padlock probes by rolling circle replication, Nucleic acids research, 26 (1998) 5073-5078.
[30] J. Wang, J. Zhang, T. Li, R. Shen, G. Li, L. Ling, Strand displacement amplification-coupled dynamic light scattering method to detect urinary telomerase for non-invasive detection of bladder cancer, Biosensors and Bioelectronics, 131 (2019) 143-148.
[31] C. He, M. Wang, X. Sun, Y. Zhu, X. Zhou, S. Xiao, Q. Zhang, F. Liu, Y. Yu, H. Liang, G. Zou, Integrating PDA microtube waveguide system with heterogeneous CHA amplification strategy towards superior sensitive detection of miRNA, Biosensors and Bioelectronics, 129 (2019) 50-57.
[32] S.-T. Han, Y. Zhou, Z.-X. Xu, L.-B. Huang, X.-B. Yang, V.A.L. Roy, Microcontact Printing of Ultrahigh Density Gold Nanoparticle Monolayer for Flexible Flash Memories, Advanced Materials, 24 (2012) 3556-3561.
[33] S. Si, W. Liang, Y. Sun, J. Huang, W. Ma, Z. Liang, Q. Bao, L. Jiang, Facile Fabrication of High-Density Sub-1-nm Gaps from Au Nanoparticle Monolayers as Reproducible SERS Substrates, Advanced Functional Materials, 26 (2016) 8137-8145.
[34] G. Song, W. Gong, S. Cong, Z. Zhao, Ultrathin Two-Dimensional Nanostructures: Surface Defects for Morphology-Driven Enhanced Semiconductor SERS, Angewandte Chemie-International Edition, 60 (2021) 5505-5511.
[35] P. Pieranski, TWO-DIMENSIONAL INTERFACIAL COLLOIDAL CRYSTALS, Physical Review Letters, 45 (1980) 569-572.
[36] A.E. Nel, L. Mädler, D. Velegol, T. Xia, E.M.V. Hoek, P. Somasundaran, F. Klaessig, V. Castranova, M. Thompson, Understanding biophysicochemical interactions at the nano–bio interface, Nature Materials, 8 (2009) 543-557.
[37] L. Liu, Y. Zhang, R. Yuan, H. Wang, Ultrasensitive Electrochemiluminescence Biosensor Using Sulfur Quantum Dots as an Emitter and an Efficient DNA Walking Machine with Triple-Stranded DNA as a Signal Amplifier, Analytical Chemistry, 92 (2020) 15112-15119.
[38] W. Bai, A. Cui, M. Liu, X. Qiao, Y. Li, T. Wang, Signal-Off Electrogenerated Chemiluminescence Biosensing Platform Based on the Quenching Effect between Ferrocene and Ru(bpy)(3)(2+)-Functionalized Metal-Organic Frameworks for the Detection of Methylated RNA, Analytical Chemistry, 91 (2019) 11840-11847.
[39] Y. Si, L. Xu, N. Wang, J. Zheng, R. Yang, J. Li, Target MicroRNA-Responsive DNA Hydrogel-Based Surface-Enhanced Raman Scattering Sensor Arrays for MicroRNA-Marked Cancer Screening, Analytical Chemistry, 92 (2020) 2649-2655.

[40] W. Zhou, Y.-F. Tian, B.-C. Yin, B.-C. Ye, Simultaneous Surface-Enhanced Raman Spectroscopy Detection of Multiplexed MicroRNA Biomarkers, Analytical Chemistry, 89 (2017) 6121-6129.
[41] Y. Si, L. Xu, T. Deng, J. Zheng, J. Li, Catalytic Hairpin Self-Assembly-Based SERS Sensor Array for the Simultaneous Measurement of Multiple Cancer-Associated miRNAs, Acs Sensors, 5 (2020) 4009-4016.
[42] Y. Su, Q. Zhang, X. Miao, S. Wen, S. Yu, Y. Chu, X. Lu, L.-P. Jiang, J.-J. Zhu, Spatially Engineered Janus Hybrid Nanozyme toward SERS Liquid Biopsy at Nano/Microscales, Acs Applied Materials & Interfaces, 11 (2019) 41979-41987.